Journal of Nuclear Materials 384 (2009) 61–69

Contents lists available at ScienceDirect

Journal of Nuclear Materials

journal homepage: www.elsevier.com/locate/jnucmat

Energetics of intrinsic point defects in uranium dioxide from electronic-structure calculations

Pankaj Nerikar [a], Taku Watanabe [a,1], James S. Tulenko [b], Simon R. Phillpot [a], Susan B. Sinnott [a,*]

[a] Department of Materials Science and Engineering, University of Florida, Gainesville, FL 32611, United States
[b] Department of Nuclear and Radiological Engineering, University of Florida, Gainesville, FL 32611, United States

ARTICLE INFO

Article history:
Received 13 August 2008
Accepted 19 October 2008

ABSTRACT

The stability range of intrinsic point defects in uranium dioxide is determined as a function of temperature, oxygen partial pressure, and non-stoichiometry. The computational approach integrates high accuracy ab initio electronic-structure calculations and thermodynamic analysis supported by experimental data. In particular, the density functional theory calculations are performed at the level of the spin polarized, generalized gradient approximation and includes the Hubbard U term; as a result they predict the correct anti-ferromagnetic insulating ground state of uranium oxide. The thermodynamic calculations enable the effects of system temperature and partial pressure of oxygen on defect formation energy to be determined. The predicted equilibrium properties and defect formation energies for neutral defect complexes match trends in the experimental literature quite well. In contrast, the predicted values for charged complexes are lower than the measured values. The calculations predict that the formation of oxygen interstitials becomes increasingly difficult as higher temperatures and reducing conditions are approached.

1. Introduction

Uranium dioxide (UO_2) is the standard fuel utilized in light water nuclear reactors. It manifests the fluorite structure at all temperatures up to its high melting point of ~3125 K [1], and can accommodate substantial quantities of fission products without significant changes in the lattice. It also maintains its useful properties in a variety of environments, and is chemically stable [2]. Intrinsic point defects are created during operation, a significant number of which persist in the fuel although many recombine or otherwise annihilate each other. Over time, these defects are detrimental to the structure and performance of the fuel, since they form defect clusters that cause fuel swelling and ultimately change the crystal structure of UO_2; this phase change is accompanied by a significant change in volume, which has highly negative effects on the microstructure and mechanical stability of the fuel pellet. These intrinsic point defects also affect the transport properties of the fission gases formed during operation, allowing them to escape from the fuel matrix and damage the fuel cladding [3]. Thus, an improved knowledge of the stability of these point defects is required for improved understanding of fuel performance.

The point defects produced include isolated vacancies and interstitials and defect complexes. These individual point defects can form these complexes in a variety of possible charged states that can influence the relative stability of a cluster. The number of possible combinations of point defects and charge states is quite large, especially since UO_2 is known to be non-stoichiometric over a wide range of compositions [4]. Any hyperstoichiometry (UO_{2+x}) or hypostoichiometry (UO_{2-x}) will stabilize some point defects in preference to others.

Theoretical calculations are complementary to experimental methods and are well-positioned to provide fundamental insight into defect chemistry [5]. This is due to the fact that systems examined computationally have well-defined compositions and the influence of each change in condition can be analyzed separately. With increases in computational resources and both more powerful and more efficient algorithms, density functional theory (DFT) can be applied to larger systems and has been successfully used to examine defect formation in numerous materials [6–10], including UO_2, with greater accuracy. For example, Petit and coworkers [11–13] used the local density approximation (LDA) and the generalized gradient approximation (GGA) to predict the energetics associated with point defect formation. Their results agree well with experimentally determined values [14]. However, their results do not predict bulk UO_2 to be an insulator. This restricts the applicability of their analysis to neutral systems [12] and prevents them from exploring the effect of charge on defect stability.

In addition to being limited to neutral defects, earlier studies were restricted to small supercell sizes. Petit et al. [13] and Freyss et al. [12] both used a 24-atom supercell owing to the high

* Corresponding author. Tel.: +1 352 846 3778; fax: +1 352 846 3355.
E-mail address: ssinn@mse.ufl.edu (S.B. Sinnott).
[1] Present address: Georgia Institute of Technology, Department of Chemical Engineering, Atlanta, GA 30332, United States.

0022-3115/$ - see front matter © 2008 Elsevier B.V. All rights reserved.
doi:10.1016/j.jnucmat.2008.10.003

computational expense of modeling UO_2. Despite these limitations, the importance of their work cannot be underestimated as these were the first calculations on UO_2 and showed that DFT could predict experimental trends successfully. With recent increases in computational power, larger system sizes have be considered. Iwasawa et al. [15] and Gupta et al. [16] each utilized the spin polarized GGA with Hubbard U correction term (SP-GGA+U) method for a 96-atom supercell and predicted the correct insulating structure of bulk UO_2. Moreover, they correctly predicted its anti-ferromagnetic ground state and found that including the correct magnetic state changes the absolute values of the formation energies of neutral point defects.

Here, we have extended this earlier work on neutral defects to include charged point defects in UO_2. We use a combination of experimental thermodynamic data and DFT calculations. The DFT calculations themselves should give the most accurate results to date, since they use the currently most sophisticated approximation within GGA, the PAW method, and 96-atom supercells, as in the previous work of Gupta et al. Most significantly, a new bridge is made between the DFT calculations and temperature, oxygen partial pressure and the charge associated with a defect, which are key parameters for controlling the type and concentration of defects. When the current and previous results on defects are considered as a whole, we see that a coherent and consistent picture of the energetics of neutral intrinsic defects is emerging. The introduction of charge leads to significant changes in these energies that vary with Fermi energy. In addition, the predicted defect formation energies of Schottky and anti-Frenkel defect complexes that consist of charged components are significantly lower than the formation energies of complexes that consist of neutral components.

The rest of this paper is organized in the following manner: Section 2 discusses the computational methods used, including the details of the determination of the defect formation energies. The results of the calculations are discussed in Section 3. It begins with the validation of the adopted approach by considering equilibrium properties, the electronic structure of UO_2, and the phase order of uranium metal (Section 3.1). Next, the formation energies of neutral point defects and defect complexes are compared with the findings of previous experimental and theoretical studies (Section 3.2). Because UO_2 exists in a wide range of experimental off-stoichiometry, the influence of charge on the relative stability of defects is investigated in Section 3.3. The effects of temperature and oxygen partial pressure are discussed in Section 3.4. Section 4 gives the conclusions of this work.

2. Computational methodology

2.1. Electronic structure calculations

The DFT calculations were performed with spin polarization by the projector augmented-wave (PAW) method [17,18] utilizing the GGA exchange correlation functional as implemented in the Vienna Ab Initio Simulation Package (VASP) [19,20]. The U $6s^2$ $6p^6$ $7s^2$ $5f^2$ $6d^2$ and O $2s^2$ $2p^4$ electrons are treated as valence electrons. We use Dudarev's simplified scheme (the so called SP-GGA+U method) [21] to include the effect of the strong correlation of 5f electrons in uranium. In addition, the values of U = 4.5 eV and J = 0.54 eV give the best match with experiment for equilibrium properties (see Table 1). Here the 5f Coulomb correlation energy (U) was determined with a combination of X-ray photoelectron spectroscopy and Bremsstrahlung isochromatic spectroscopy [23] and the onsite exchange energy (J) was determined using X-ray photoemission spectroscopy [21]. This leads to a U_{eff} value of 3.96 eV and hence we have chosen this value. These values are similar to those previously used by others [15,16,21,22] and also to experimental measurements [23].

UO_2 is experimentally known to be anti-ferromagnetic below 30 K [22], and this state has been taken for our calculations. With regard to other calculation parameters, we used a $1 \times 1 \times 1$ unit cell for our initial tests. The Brillouin zone sampling used a $4 \times 4 \times 4$ Monkhorst-Pack k-point mesh [24], and the cut-off energy for the plane waves was 400 eV. The combination of the above parameters resulted in a lattice parameter of 0.549 nm and a band gap of 1.92 eV, both of which are in good agreement with experiment (see Table 1).

A $2 \times 2 \times 2$ unit cell was then used for the pristine and defect-containing structures for the defect energy calculations. In the case of the pristine supercell, cell shape and atomic positions were relaxed to their equilibrium positions. However, in the case of the supercells that contained point defects only the atomic positions were relaxed while the cell shape was kept fixed. This is critical for defect calculations in the limit of dilute defect concentrations [25], since allowing the cell volume to relax corresponds to calculating the lattice constant of a system with a high concentration of defects (the actual defect concentration within the supercell), which is not the objective of this work.

2.2. Defect formation energy

The formation energy of a defect as a function of temperature, partial pressure, defect species α, and charge state q is given as follows [25]:

$$\Delta G_f(\alpha, q, T, P) = E^{\text{total}}(\alpha, q) - E^{\text{total}}(\text{perfect}) - \sum n_i \mu_i(T, P) + q[E_F + E_V + \Delta V], \quad (1)$$

here $E^{\text{total}}(\alpha, q)$ is the optimized energy of the supercell containing the defect α of charged state q, and E^{total} (perfect) is the optimized energy of the perfect supercell. Both these values are obtained directly from the DFT calculations. In Eq. (1), n_i represents the number of atoms of species i added to ($n_i > 0$) or subtracted from ($n_i < 0$) the system; μ_i is the chemical potential of species i. The last term is seen as an electronic chemical potential that represents the change in energy associated with charged defects. In this term, E_F is the Fer-

Table 1
The calculated properties of bulk uranium oxide are shown using different approximations. These values are compared to published experimental and theoretical data. It is to be noted that experimentally, the lattice parameter was reported at room temperature while the ab initio calculation data are determined at 0 K.

	Method	Lattice parameter (nm)	Band gap (eV)	Magnetic moment (μB)
Experiment [1,23]		0.547	2.00	1.74
Freyss [12]	GGA	0.540	0.00	0.00
Dudarev [21]	LMTO-LSDA+U	0.537	2.10	1.70
Gupta [16]	PAW-SP-GGA+U	0.552	1.80	1.94
This work	LDA	0.526	0.00	0.00
	GGA	0.533	0.00	0.00
	LSDA	0.530	0.00	–
	SP-GGA	0.542	0.00	–
	LSDA+U	0.543	1.68	–
	PAW-SP-GGA+U	0.549	1.92	1.93

mi level in the bulk with reference to the valence band maximum and E_V is the energy of the bulk valence band maximum. Since we use the bulk value of the valence band maximum to estimate the energy of a defect supercell, the electrostatic potential of the defective structure has to be aligned with the bulk value; the term ΔV represents this alignment.

The Fermi energy is treated as a variable in this approach and is dependent upon the charge associated with the cumulative effect of defects and dopants in the system. A physically meaningful range around the Fermi energy of pristine UO_2 is considered. The vibrational entropy is neglected; we have previously demonstrated in the context of TiO_2 that such vibrational contributions are small [26]. The configurational entropy is treated within the ideal solution model [9].

2.3. Thermodynamic component

The chemical potential μ_i (T, P) is also treated as a variable in our calculations. Following the approach of He et al. [26,27], the oxygen chemical potential in UO_2 is expressed as follows:

$$\mu_O(T,P) = \frac{1}{2}\left[\mu^0_{UO_2} - \mu^0_U - \Delta^0_{f,UO_2}\right] + \Delta\mu^0_O(T) + \frac{1}{2}k_B T \ln\frac{P}{P^0}, \qquad (2)$$

where $\mu^0_{UO_2}$ and μ^0_U are the chemical potentials of bulk UO_2 and uranium metal as calculated with DFT. Uranium metal forms three phases with increasing temperature [1]. The parameters U and J were kept constant while calculating the chemical potentials of these phases. $\Delta G^0_{f,UO_2}$ is the Gibbs energy per mole of UO_2 under standard conditions obtained from thermodynamic data [28], and $\Delta\mu^0_O$ (T) is the change in oxygen chemical potential with change in temperature obtained from thermodynamic data [28]. Thus, Eq. (2) allows us to calculate a chemical potential of oxygen that varies in a physically meaningful way with temperature and oxygen partial pressure; this would not have been possible if this chemical potential had been calculated directly from a DFT calculation of an oxygen molecule that is, by definition, carried out at zero Kelvin in perfect vacuum.

Thus, the combination of Eqs. (1) and (2) allows us to consider the effect of system conditions on the defect formation energies obtained through DFT calculations.

3. Results and discussion

3.1. Equilibrium properties of bulk UO_2 and uranium metal

The first step to validate our approach is to calculate the lattice parameter and band gap of bulk UO_2 using different

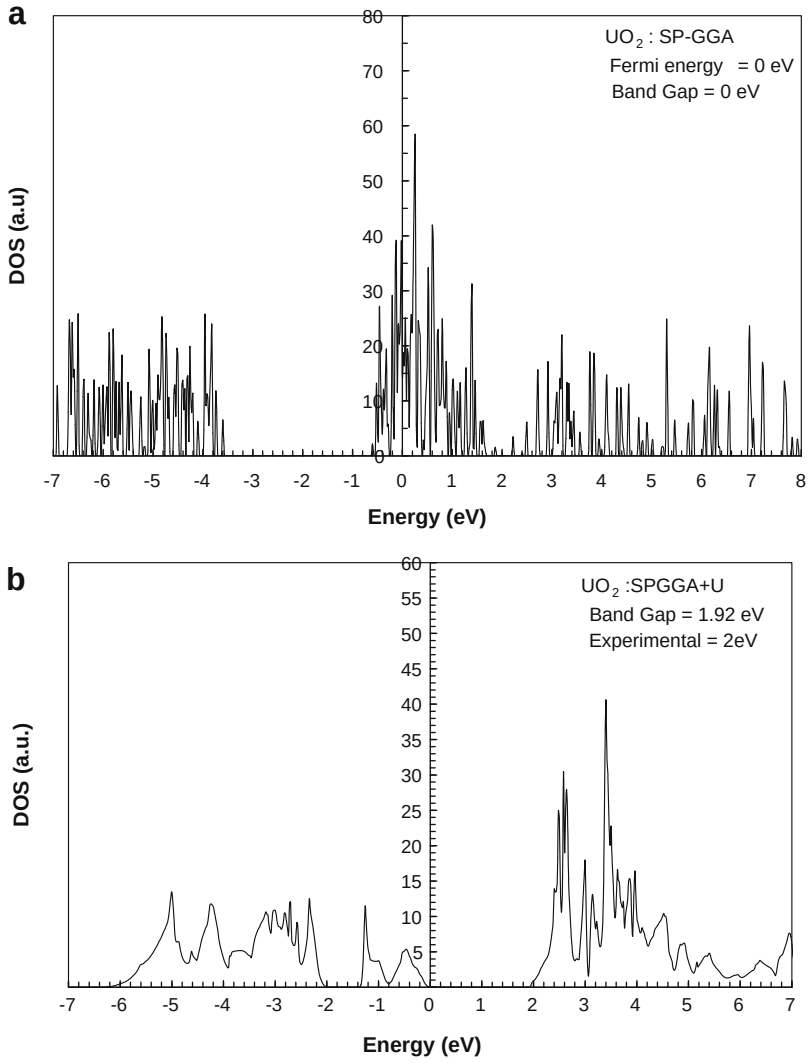

Fig. 1. Total DOS projected to the U 5f and 6d orbitals as the conduction band and to the U 5f and O 2p as the valence band for antiferromagnetic UO_2 using (a) SP-GGA, or (b) SP-GGA+U method. The energy on the x axis is with reference to the Fermi level. Notice that the inclusion of spin by itself does not result in a band gap for GGA.

pseudopotentials. Table 1 compares the lattice parameter, the band gap and the magnetic moment of the uranium ion from published computational and experimental work with values calculated using various approximations within DFT. We find that the agreement with the experimental lattice parameter improves as these approximations become more sophisticated. For example, pure LDA and GGA give the poorest agreement with experiment, but the agreement significantly improves with the addition of spin polarization. Of all the methods considered, the PAW-SP-GGA+U method gives the best match with experimental data, even though it tends to overestimate the lattice parameter slightly. Our results are similar to the PAW-SP-GGA+U results of Gupta et al. [16]; the small discrepancy between the two sets of results most probably arises from the slight differences in the value of U_{eff} ($U - J$) used in the calculations (we used a value of 3.96 eV for U_{eff} and Gupta et al. used a value of 4.00; both values fall within the experimentally determined range [23]).

Uranium dioxide is an electrical insulator [23]; however, DFT predicts it to be a metal unless the 5f electron on site repulsion is included using in the +U term (refer to Table 1). Fig. 1 shows the density of states (DOS) plots calculated from PAW-SP-GGA and PAW-SP-GGA+U calculations. While the former predicts UO_2 to be metallic, the latter gives a band gap of 1.92 eV, which is only 0.08 eV smaller than the experimental value. More detailed analysis shows that the valence band consists mainly of U 5f and O 2p orbitals while the conduction band (Fig. 1(b)) is mainly derived from 6d and 5f orbitals. In the PAW-SP-GGA method, all of these orbitals are clustered together leading to the metallic state shown in Fig. 1(a).

The spin polarization of the U 5f orbital controls the anti-ferromagnetic ground state. Our calculations take this effect into account. The magnetic moment of each uranium ion is predicted to be 1.93 μ_B, a value that is about 10% larger than the experimental value. Of course, the net magnetization is 0 as should be the case for an anti-ferromagnetic material. This correct description of the electronic state gives us confidence that this method will be able to correctly describe charged defects. The different charges associated with a defect affect the Fermi level (E_F) and therefore influence the relative stability of the charged defect relative to the neutral defect; this will be discussed in more detail in Section 3.3.

One of the goals of this work is to predict the role of temperature on point defect formation. Bulk uranium metal exists in three different phases α, β and γ, depending on temperature. The α-phase is the most stable phase under ambient conditions and has an orthorhombic crystal structure with four atoms per unit cell. The β-phase, which is stable at intermediate temperatures, has a body-centered tetragonal structure; the highest temperature γ-phase has a body-centered cubic structure. The PAW-SP-GGA+U calculations predict this phase order correctly, as indicated in Table 2. This provides further validation for this approach and is also critical for predicting the effect of temperature on defect formation energies from Eq. (1). However, we should point out that we did not do the corresponding calculations for the other DFT approximations. These calculations have been carried out previously by Freyss et al. [12] who also found the correct phase order.

Table 2
Relative stabilities of the three different phases of bulk uranium metal, the orthorhombic α-phase, the body-centered tetragonal β-phase, and the body-centered cubic γ-phase. Predicting the correct phase order is important for the defect energy calculations. The SP-GGA+U method was used in these calculations to obtain a consistent reference state.

Phase	Temperature range (K)	μ_U (eV/atom)
α-U	Up to 941	−8.08
β-U	941–1049	−7.93
γ-U	1049–1408	−7.57

These initial calculations of lattice parameter, band gap, magnetic moment and phase order agree well with experiment and give us confidence that the PAW-SP-GGA+U approach will be appropriate for defect energy calculations.

3.2. Formation energy of neutral defects

Although DFT has been found to accurately describe the energetics of neutral defects, it is still limited to a relatively small number of atoms and electrons in the system. UO_2 is especially challenging for DFT because it has a large number of electrons, strong electron-electron correlations, and is anti-ferromagnetic, all of which must be included to properly model the material. Our calculations therefore use a $2 \times 2 \times 2$ supercell, which is effectively the current system-size limit for such calculations. This limitation on system size is important as there could be interactions between periodic images of the defect in neighboring supercells. To estimate the effects of the limited supercell size used, defect calculations were also carried out using an empirical potential within the general utility lattice program (GULP) [29,30]. The advantages of this approach are that larger supercell sizes can be treated at a small fraction of the computational cost of DFT calculations. The calculated values are less accurate than those obtained with DFT, but the effects of supercell size are not expected to change significantly with method. We have chosen the Yamada potential [31] for these GULP calculations. This potential includes partial charges and a Morse term to model covalent character. It yields more accurate values for energetics of point defects than most other potentials [32]. The normalized defect formation energies of the anti-Frenkel, Frenkel and the Schottky defects are plotted in Fig. 2.

The defect energy converges as we increase the system size. For the anti-Frenkel and the Schottky defects, the energy is almost converged as the size of the supercell is increased to $2 \times 2 \times 2$. For the Frenkel defect, the change in the defect energy is ≈12% between the $2 \times 2 \times 2$ and $3 \times 3 \times 3$ supercells and changes very little (≈5%) beyond this as the system size increases further. Based on this analysis, we can anticipate that defect energies calculated using DFT for the $2 \times 2 \times 2$ should be accurate to about 7%, except in the case of the Frenkel defect, where the uncertainty is about 10%.

All the point defects whose formation energies have been reported so far in the literature from DFT calculations have been neutral. For the sake of completeness, and to unify the sometimes dissimilar literature values, we therefore also calculate the forma-

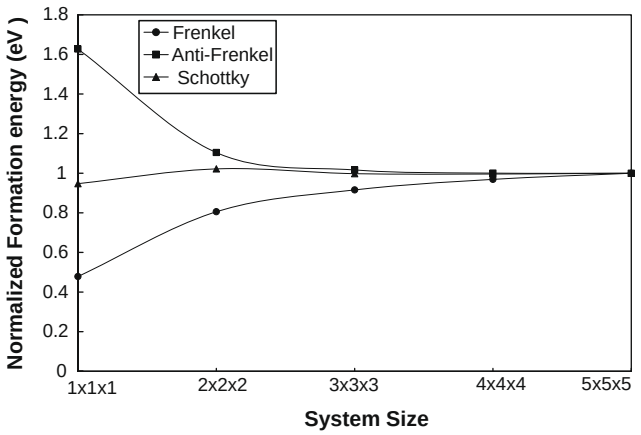

Fig. 2. Normalized formation energy of neutral defect complexes calculated as a function of system size by atomic level simulations using an empirical potential within GULP. The system sizes are multiples of the primitive fluorite cell along the x, y and z directions. The energies have been normalized with respect to the $5 \times 5 \times 5$ system.

Table 3
Calculated formation energies of neutral point defects compared to reported work using various approximations.

	Method	Oxygen vacancy (eV)	Oxygen interstitial (eV)	Uranium vacancy (eV)	Uranium interstitial (eV)	System size
Freyss [12]	GGA	6.1	−2.5	4.8	7.0	$2 \times 1 \times 1$
Crocombette [11]	LDA	6.7	−2.9	3.3	7.3	$2 \times 1 \times 1$
Gupta [16]	PAW-SP-GGA+U	5.6	−1.6	6.0	8.2	$2 \times 2 \times 2$
Iwasawa [15]	PBE-SP-GGA+U	4.46	−0.44	8.45	4.70	$2 \times 2 \times 2$
This work	PAW-SP-GGA+U					$2 \times 2 \times 2$
	Ref. state: α-U	4.32	−0.37	8.96	6.12	
	Ref. state: O_2	5.29	−1.34	7.04	8.04	

tion energies associated with neutral uranium and oxygen vacancies and interstitials. We compare our findings to published results in Table 3. The qualitative trend predicted by all the calculations is the same. In particular, they all predict that the oxygen interstitial has negative formation energy. This suggests that UO_2 is unstable in the presence of oxygen vapor, which is consistent with the fact that UO_2 is well-known to be hyperstoichiometric [14]. The large positive formation energy for O vacancies is also consistent with the very narrow range of stability of hypostoichiometric UO_2.

Although the various methods agree on the order of stability of the defects, they do not agree on the absolute values of defect formation energies. There could be a number of possible reasons for this. Some calculations [11,12] used pure GGA as their exchange correlation functional while others used SP-GGA+U [15,16]. In the SP-GGA+U methods, a spin polarized, anti-ferromagnetic state was considered while in the GGA calculations a non-spin polarized and non-magnetic state was considered. Even when the same exchange correlation functional was used, differences in the results are most likely due to the fact that different types of pseudopotentials were used. For example, Iwasawa [15] used the PBE-SP-GGA+U pseudopotential while Gupta et al. [16] utilized the PAW-SP-GGA+U pseudopotential; the latter is expected to be the more accurate. Importantly, Iwasawa allowed the defect-containing supercell to relax under constant pressure (approximating the high defect concentration limit), while Gupta et al. performed a constant volume calculation that approximates the low concentration limit. We also performed constant volume calculations. Considering the similarities between our approach and the approach of Gupta et al., it is not surprising that our defect formation energies are in reasonable agreement.

Table 3 further indicates that the choice of the reference state for the defect calculations is important. Freyss et al. [12] used a reference state of α-uranium for uranium defects and an oxygen molecule for oxygen defects, where in each case the reference state chemical potential was calculated directly with DFT. This approach is valid when one is not considering distributed Schottky defects or the effect of temperature and pressure on defect formation energies. In this work, however, our goal is to investigate the effect of temperature and partial pressure on defect energies. We have therefore adopted the slightly different approach embodied in Eqs. (1) and (2). Thus, when α-uranium is the reference state we calculate its chemical potential with DFT. We then determine the chemical potential of oxygen (μ_O) using Eq. (2), which allows us to consider the effect of temperature and oxygen partial pressure on defect formation energies. The justification for this choice is that temperature and atmospheric pressure have a greater influence on the chemical potential of gaseous oxygen than on solid α-uranium. However, if we use an oxygen molecule as the reference state, calculate its chemical potential with DFT, and obtain the chemical potential of uranium (μ_U) from Eq. (2), we obtain somewhat different values for defect formation energies, as indicated in Table 3. Although this choice of reference state changes the values of the formation energies, it does not affect the qualitative picture that the formation energy for neutral oxygen interstitials is negative, the formation energy for oxygen vacancies is large, and those for uranium defects are even larger.

The individual point defect formation energies in Table 3 can be combined to explore the relative stability of neutral defect complexes in UO_2, which can be compared more directly with experiment. Such a calculation corresponds to all of the point defects being dissociated from one another and at a sufficient distance apart that they do not interact; this thus ignores association energies. The experimental values in Table 4 are reported as a range, indicative of the difficulty associated with measuring absolute values. The calculated values are in good agreement with experiment for the anti-Frenkel pair and are quite reasonable for the Schottky defect. However, the calculated values for the formation energy of the Frenkel defect are significantly larger than the experimental value. This might be attributable to the fact that the Frenkel formation energy was determined indirectly in experiment from oxygen diffusion data; indeed it has been suggested that the experimentally measured value is an underestimate [32].

A similar calculated and experimental trend is observed in other fluorites such as PuO_2, ThO_2 and CaF_2 where the anti-Frenkel defect is found to dominate (Table 4). The calculations were carried out using empirical potentials and oxygen diffusion experiments were carried out for the anti-Frenkel formation energies. The data cited in the table is limited to the dominant defects in each system. The actual values for the anti-Frenkel defect are also rather similar to that for UO_2.

Table 4
The values for Frenkel energies are given for different compounds having the fluorite structure. The comparison indicates that the anti-Frenkel is the dominant defect for all compounds with the fluorite structure and is not limited to actinide oxides. The formation energies were calculated assuming the individual point defects are far apart, neutral, and non-interacting.

	Method	Anti-Frenkel (eV)	Frenkel (eV)	Schottky (eV)	Melting temperature (K)
Experiment [1,14]		3.0–4.6	8.5–9.6	6.0–7.0	3125
Freyss [12]	GGA	3.6	11.8	5.6	
Crocombette [11]	LDA	3.8	10.6	5.8	
Gupta [16]	PAW-SP-GGA+U	4.0	14.2	7.2	
This Work	PAW-SP-GGA+U	3.95	15.08	7.6	
CaF_2 [1,37]	Oxygen diffusion	2.7	–	–	1691
PuO_2 [1,35]	Oxygen diffusion	2.7–2.9	–	–	2740
ThO_2 [1,35]	Oxygen diffusion	2.3–4.7	–	–	3663

3.3. Effect of charged states

It is usual to think of point defects in metal oxides as being charged rather than neutral. For example, when an oxygen vacancy is created it is considered to carry a charge of +2 in traditional Kröger-Vink notation, which represents the loss of two electrons. However, most calculations of the formation energies of point defects, such as those discussed in the previous section, treat them as neutral. In this section we explore the effects of charge on the formation energy of the defect. This is done by explicitly applying charge to the supercell, some of which is localized around the defect, while, as is usual for DFT, most is distributed throughout the supercell in a manner that is representative of delocalization. The influence of charge on the defect formation energy is taken into account in two places in Eq. (1). The first is through the DFT calculation of the charged, defect-containing supercell and the other is through the electron chemical potential term, which effectively shifts the Fermi energy. For example, for an n-type defect the Fermi level will be near the conduction band, while for a p-type defect it will be near the valence band. The most stable defect is that for which the defect energy is lowest for a specific Fermi level.

This is illustrated in Fig. 3, which compares the energies associated with forming V_O^x, $V_O^{\bullet}$, and $V_O^{\bullet\bullet}$ oxygen vacancies. A transition can be observed as the Fermi level is increased from the valence band (0.0 eV) to the conduction band (1.92 eV). Close to the valence band, the +2 charged oxygen vacancy is favored. This in turn means that oxygen vacancies have a tendency to donate electrons or behave as an n-type defect. With an increase in Fermi level up to 0.6 eV, the +1 charged oxygen vacancy becomes energetically favorable. With further increases in the Fermi level, the tendency of the oxygen vacancy to donate electrons diminishes and the neutral oxygen vacancy becomes dominant as the Fermi level approaches the conduction band.

The energies of all the individual point defects considered are shown in Fig. 4 as a function of the position of the Fermi energy. When considering only the vacancy defects, the +2 charged oxygen vacancy is predicted to be the most stable defect near the valence band. This in turn predicts that even in the presence of a uranium vacancy, which is a p-type defect, the system will still donate electrons. However, as the Fermi level approaches the conduction band, the −4 charged uranium vacancy becomes increasingly favorable and remains the dominant defect over the range from 0.3 to 2.0 eV. When considering only differently charged uranium vacancies, the −4 charged vacancy is the most favorable. The formation energy of this charged vacancy is significantly lower than

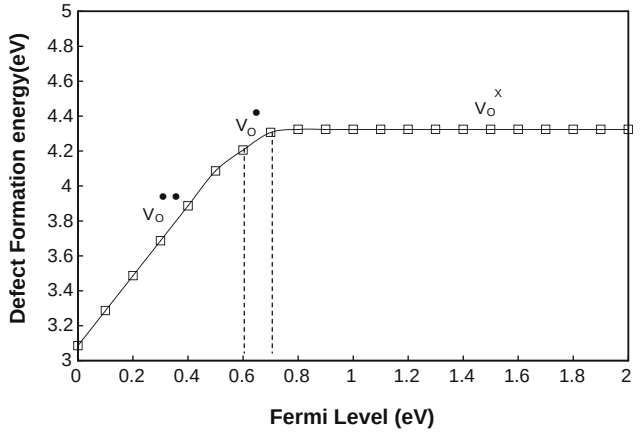

Fig. 3. Stability transitions for the neutral, +1 and +2 charged oxygen vacancies as a function of Fermi level over the entire band gap. Only the most dominant defect with reference to a particular Fermi level is shown for clarity.

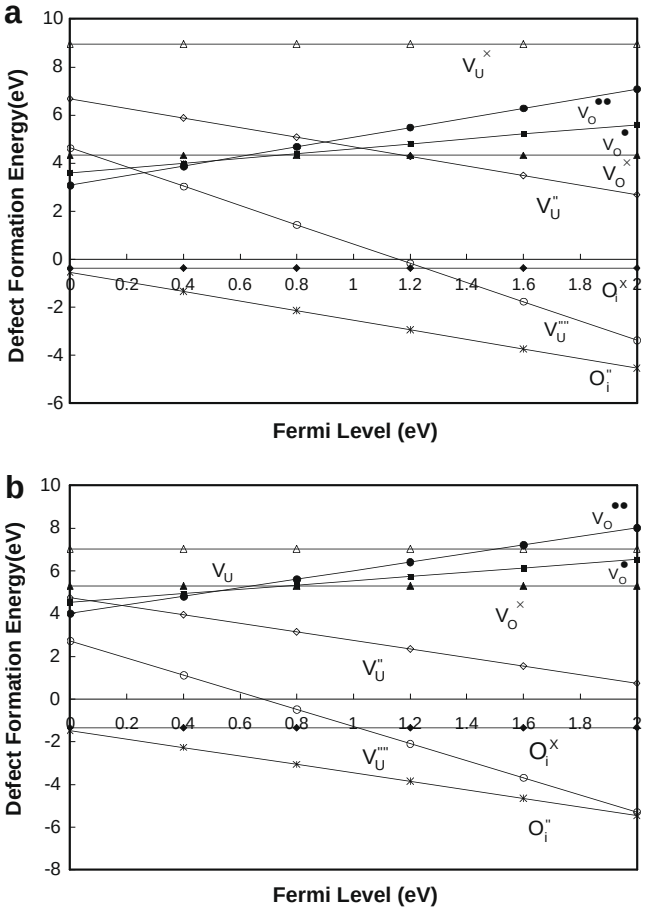

Fig. 4. Calculated defect formation energies for variously charged oxygen and uranium point defects as function of reference state (a) α-uranium, (b) oxygen molecule. The empty symbols denote uranium while the filled symbols and other are oxygen.

that of the neutral vacancy. We also examined the effect of charge on the oxygen interstitial (see Fig. 4). We did not consider the effect of charge on uranium interstitials because the formation energy of the Frenkel pair is so high. Finally, we observe that the −2 charged oxygen interstitial (O_i'') dominates over the entire range of the Fermi energies considered, but increases in stability as the Fermi energy approaches the conduction band. Using the same formalism as in Section 3.2, we can simulate the effect of stoichiometry by choosing different reference states. Choosing α-uranium as the reference state (Fig. 4(a)) would correspond to a hypostoichiometric (UO_{2-x}) case while choosing an oxygen molecule as a reference (Fig. 4(b)) corresponds to a hyperstoichiometric (UO_{2+x}) case. The former reference state would shift the Fermi level towards the conduction band and the latter would shift it towards the valence band. We observe that the changes in environmental conditions do not affect the general conclusions. However, there are changes in quantitative trends when comparing both cases. The formation energy of an oxygen vacancy is significantly lower in the hypostoichiometric case as it is easier to form an oxygen vacancy in an oxygen deficient scenario. On the other hand, it becomes easier to form an oxygen interstitial and a uranium vacancy when an oxygen molecule is considered to be the reference, as both these defects contribute to the hyperstoichiometry in the system.

This analysis of the relative stabilities and behavior of individual point defects is informative. However, point defects do not occur in isolation but rather in combinations, such as Frenkel,

anti-Frenkel and Schottky complexes [32]. We therefore now compare the energies associated with complexes that consist of either a combination of neutral or charged defects. Because the complexes are charge neutral, the position of the Fermi level does not enter the calculations, even though the energy of the individual charged defects varies with the Fermi level. The formation energy of the anti-Frenkel complex is given in Fig. 5. It is clear that the charges on the individual defects that make up the complex influence its overall formation energy, an effect previously predicted for TiO_2 [26]. Specifically, the combination of an oxygen anti-Frenkel pair of charged defects ($V_O^{\bullet\bullet} + O_i''$) has a lower formation energy than the corresponding combination of neutral point defects ($V_O^x + O^x$). However, as discussed in Section 3.2, the calculated formation energy for a Frenkel complex made from neutral defects agrees reasonably well with experimental measurements. Thus the combination of charged components yields a formation energy that is considerably lower than the experimental value. The reasons for this remain unresolved, but could be due in part to the neglect of association energies or the way in which DFT distributes charge within the supercell.

A similar trend is seen for the Schottky defects, which are illustrated in Fig. 6. The formation energy of the Schottky defect as a combination of charged vacancies ($V_U^{\bullet\bullet} + 2V_O^{\bullet}$) is significantly lower (≈50%) than the combination of neutral vacancies. As for the anti-Frenkel, the calculated energy of the Schottky defect of neutrals components also agreed reasonably well with experiment.

The difference in energy between the anti-Frenkel and Schottky defects is predicted to vary considerably with charge. This is because the uranium vacancy is affected to a greater degree than the oxygen point defects (see Fig. 4) when charges associated with the constituent point defects are considered. This phenomenon can be seen as a consequence of the strong electron correlation of the uranium atom, in addition to the factors listed above for the charged anti-Frenkel defect complex.

3.4. Effect of temperature and oxygen partial pressure

The typical operating conditions of a nuclear reactor span a variety of temperatures and oxygen partial pressures. The influence of temperature on the defect formation energies is discussed first in Fig. 7. The temperature range considered is from 300 to 1400 K at standard atmospheric pressures of 1 atm. This range was specifically chosen after examining the phase diagram in order to observe the effect of temperature on the stoichiometry of the fuel [33]. In general, UO_2 is hyperstoichiometric but this tendency

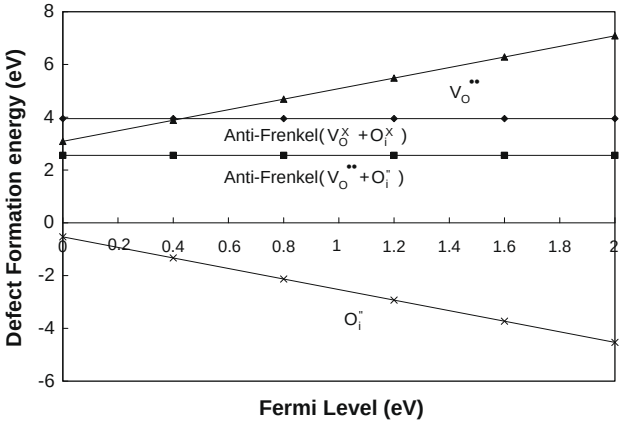

Fig. 5. Calculated formation energy of the anti-Frenkel defect as a function of the Fermi level; the formation energies of the neutral complexes are compared to charged individual defects.

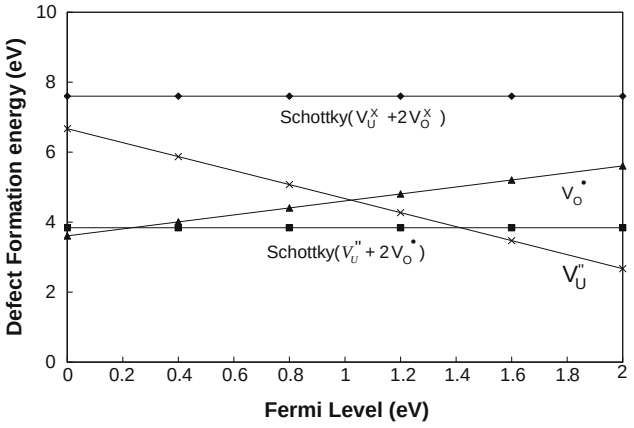

Fig. 6. Calculated formation energy of the Schottky defect as a function of the Fermi level; the formation energies of the neutral complexes are compared to charged individual defects.

decreases as the temperature increases; hypostoichiometry exists in measurable quantities only at high temperatures.

The oxygen interstitial is still predicted to be the dominant defect present. However, the formation energy of this defect increases as the temperature increases. This observation in turn means that the formation energy of an oxygen vacancy should decrease with temperature, which is consistent with the narrowing of the hyperstoichiometric range. This trend is indeed seen in the calculations, where the oxygen point defects are more energetically favorable than their uranium counterparts. The calculations also indicate that the uranium defects are affected to a greater degree by the phase transitions of bulk uranium with temperature. In particular, the formation energy of the uranium vacancy decreases while that of the uranium interstitial increases as temperature increases.

The other significant issue is the equilibrium pressure of oxygen within the fuel which, to a substantial degree, determines whether the fuel will oxidize the metallic cladding surrounding it [34]. This leads to an undesirable thinning of the cladding. In Fig. 8, the effect of oxygen partial pressure on the defect formation energies at 800 K is shown. This temperature was specifically chosen because it is the rim temperature of a typical UO_2 pellet in an LWR. Additionally, many experiments have been carried out in the partial pressure range used here, which allows our predictions to be readily correlated with experimental results [33].

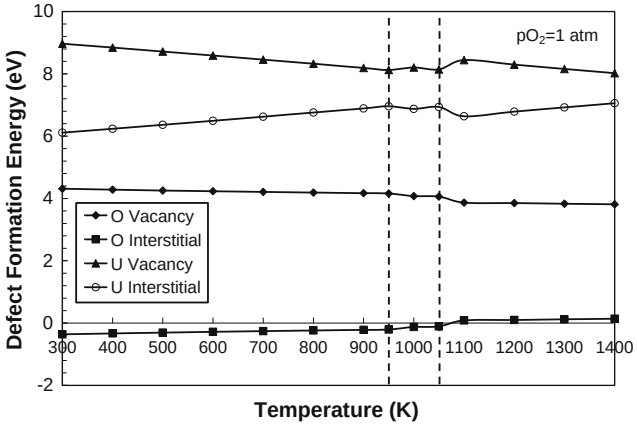

Fig. 7. Predicted effect of temperature on the formation of neutral point defects at standard atmospheric pressure for the temperature range of 300 to 1400 K. The vertical dashed lines indicate a phase change of bulk uranium metal, which is an integral part of our model.

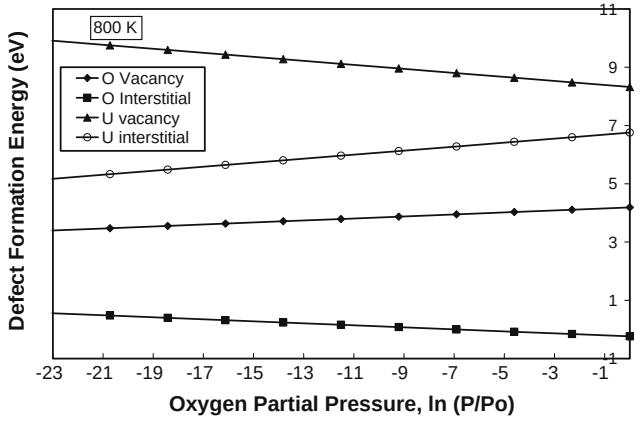

Fig. 8. Predicted effect of oxygen partial pressure on the formation of neutral point defects in UO_2 at 800 K; the partial pressure of oxygen is varied from $p_{O2} = 1 \times 10^{-10}$ atm. to 1 atm. This corresponds to highly reducing and oxidizing conditions.

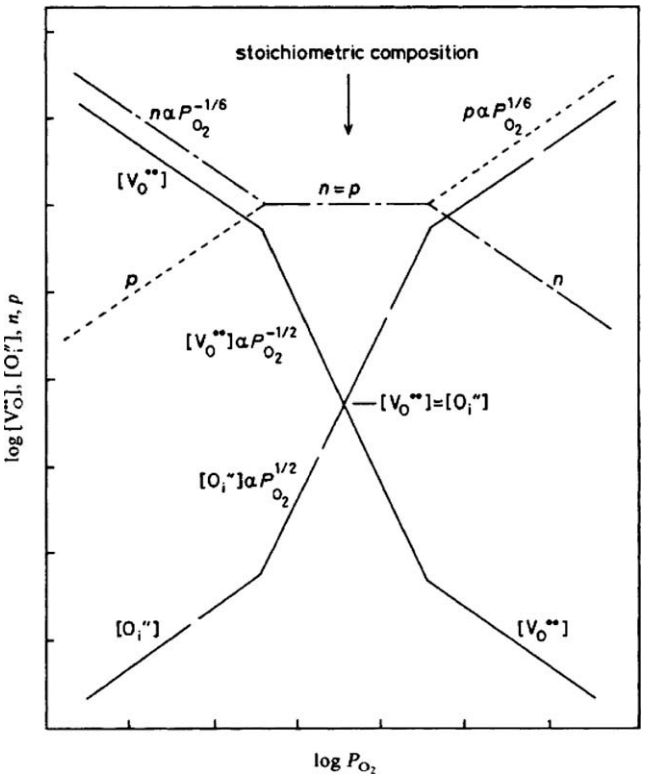

Fig. 9. Brouwer diagram for UO_{2+x} adopted from Murch et al. [35]. The diagram assumes that the intrinsic electronic reaction dominates and neglects defects on the uranium sub-lattice.

This thermodynamic analysis predicts the oxygen interstitial to be the most stable point defect. However, it becomes increasingly difficult to form this defect as the partial pressure is reduced. This is expected as at highly reduced conditions there is little free oxygen in the system and the tendency to lose oxygen to the atmosphere is significant. On the other hand, it becomes energetically feasible to form oxygen vacancies in reducing conditions. This contrasting nature of oxygen can be understood on the basis of the Brouwer's diagram for UO_2 in Fig 9 where the concentration of defects is plotted as a function of oxygen partial pressure [35]. As indicated in the figure, the concentration of oxygen vacancies is proportional to $p_{O_2}^{-1/2}$ which accounts for their being energetically unfavorable at high oxygen partial pressures. The decrease in oxygen vacancy concentration increases the uranium vacancy concentration. Furthermore, the formation energy of the cation vacancy drops dramatically as the oxygen partial pressure increases. This is due to the fact that Schottky equilibrium [36] or charge neutrality through vacancies must be maintained in the system.

4. Conclusions

In this work, a combined electronic-structure DFT and thermodynamic approach has been used to predict the stability of intrinsic point defects in UO_2. These calculations were supplemented by empirical potential-calculations using larger supercells. The electronic structure and equilibrium structure of UO_2 are well reproduced. The formation energies of individual point defects are seen to depend on the exchange-correlation functional chosen within the DFT calculations, whether the defect-containing supercell was allowed to relax or not, and on the chosen reference state chemical potential. The DFT and empirical potential calculated formation energies for neutral defect complexes match both qualitative and quantative trends reported in the literature in that the oxygen Frenkel pair is predicted to be the most stable defect overall.

The stability of charged defects was also analyzed by taking into account the various charge states they are known to possess. The +2 charged oxygen vacancy was predicted to be dominant when the Fermi level is near the valence band, but the −4 charged uranium vacancy was predicted to become the energetically favored defect as the Fermi level moves towards the conduction band. The stability of the anti-Frenkel and Schottky defect complexes depend to a significant degree on whether the individual point defects that made them up were charged or neutral. The formation energies of the neutral complexes agree better with the experimental values than the energies of the charged complexes for reasons that are, at this point, unresolved.

The influence of temperature and partial pressure was also analyzed. In general, the oxygen interstitial remains dominant over the entire range of oxygen partial pressures; however, it becomes increasingly difficult to form these defects as we approach higher temperatures and reducing conditions. These predictions are consistent with experimental observations and measurements.

Acknowledgements

We are happy to acknowledge support for this work through DOE-NERI Award DE-FC07-05ID14649 and the DOE-BES computational materials science network. We also thank the high performance computing (HPC) at the University of Florida for providing resources for the density functional theory calculations.

References

[1] P. Villars, L.D. Calvert (Eds.), Pearson's Handbook of Crystallographic Data for Intermetallic Phases, ASM, Metals Park, Ohio, 1985.
[2] C. Sari, U. Benedict, H. Blank, J. Nucl. Mater. 35 (1970) 267.
[3] R.W. Grimes, C.R.A. Catlow, Philos. Trans. Roy. Soc. A 335 (1991) 609.
[4] C.R.A. Catlow, J. Nucl. Mater. 79 (1979) 432.
[5] M.C. Payne, M.P. Teter, D.C. Allan, T.A. Arias, J.D. Joannopoulos, Rev. Mod. Phys. 64 (1992) 1045.
[6] M. Stan, J.C. Ramirez, P. Cristea, S.Y. Hu, C. Deo, B.P. Uberuaga, S. Srivilliputhur, S.P. Rudin, J.M. Wills, J. Alloy. Compd. 444 (2007) 415.
[7] A.E. Mattsson, P.A. Schultz, M.P. Desjarlais, T.R. Mattsson, K. Leung, Model. Simul. Mater. Sci. 13 (2005) R1.
[8] P. Erhart, A. Klein, K. Albe, Phys. Rev. B 72 (2005) 085213.
[9] A.F. Kohan, G. Ceder, D. Morgan, C.G. Van de Walle, Phys. Rev. B 61 (2000) 15019.
[10] S.K. Xiang, H.C. Huang, L.M. Hsiung, J. Nucl. Mater. 375 (2008) 113.
[11] J.P. Crocombette, F. Jollet, L.N. Nga, T. Petit, Phys. Rev. B 6410 (2001) 104107:1.
[12] M. Freyss, T. Petit, J.P. Crocombette, J. Nucl. Mater. 347 (2005) 44.

[13] T. Petit, C. Lemaignan, F. Jollet, B. Bigot, A. Pasturel, Philos. Mag. B 77 (1998) 779.
[14] H. Matzke, J. Chemical Society, Faraday Trans. II 83 (1987) 1121.
[15] M. Iwasawa, Y. Chen, Y. Kaneta, T. Ohnuma, H.Y. Geng, M. Kinoshita, Mater. Trans. 47 (2006) 2651.
[16] F. Gupta, G. Brillant, A. Pasturel, Philos. Mag. 87 (2007) 2561.
[17] P.E. Blochl, Phys. Rev. B 50 (1994) 17953.
[18] G. Kresse, D. Joubert, Phys. Rev. B 59 (1999) 1758.
[19] G. Kresse, J. Furthmuller, Phys. Rev. B 54 (1996) 11169.
[20] G. Kresse, J. Hafner, Phys. Rev. B 47 (1993) 558.
[21] S.L. Dudarev, D.N. Manh, A.P. Sutton, Philos. Mag. B 75 (1997) 613.
[22] R. Laskowski, G.K.H. Madsen, P. Blaha, K. Schwarz, Phys. Rev. B 69 (2004) 140408.
[23] Y. Baer, J. Schoenes, Solid State Commun. 33 (1980) 885.
[24] H.J. Monkhorst, J.D. Pack, Phys. Rev. B 13 (1976) 5188.
[25] C.G. Van de Walle, J. Neugebauer, J. Appl. Phys. 95 (2004) 3851.
[26] J. He, R.K. Behera, M.W. Finnis, X. Li, E.C. Dickey, S.R. Phillpot, S.B. Sinnott, Acta Mater. 55 (2007) 4325.
[27] M.W. Finnis, A.Y. Lozovoi, A. Alavi, Annu. Rev. Mater. Res. 35 (2005) 167.
[28] I. Barin (Ed.), Thermochemical Data of Pure Substances, Part II, VCH, Berlin, 1989.
[29] J.D. Gale, J. Chemical Society, Faraday Trans. 93 (1997) 629.
[30] J.D. Gale, A.L. Rohl, Mol. Simulat. 29 (2003) 291.
[31] K. Yamada, K. Kurosaki, M. Uno, S. Yamanaka, J. Alloy. Compd. 307 (2000) 10.
[32] K. Govers, S. Lemehov, M. Hou, M. Verwerft, J. Nucl. Mater. 366 (2007) 161.
[33] B.J. Lewis, W.T. Thompson, F. Akbari, D.M. Thompson, C. Thurgood, J. Higgs, J. Nucl. Mater. 328 (2004) 180.
[34] D.R. Olander, Fundamental Aspects of Nuclear Reactor Fuel Elements, Tech. Info. Division, U.S. Dept. of Energy, 1976.
[35] G.E. Murch, C.R.A. Catlow, J. Chemical Society, Faraday Trans. II 83 (1987) 1157.
[36] M.W. Barsoum, Fundamentals of Ceramics, McGraw-Hill Companies, 1997.
[37] C.R.A. Catlow, M.J. Norgett, J. Phys. C 6 (1973) 1325.